

Modeling Supersonic Combustion

C. Fureby[†] & V. Sabel'nikov[‡]

[†]Defense Security Systems Technology, The Swedish Defense Research Agency – FOI,
147 25, Tumba, Stockholm, Sweden

[‡]Fundamental and Applied Energetics Department, ONERA,
Chemin de la Hunière, 91761 Palaiseau Cedex, France

1 Introduction and Background

Supersonic combustion is encountered in many applications including scramjets and dual-mode ramjets, pulse detonation engines, continuous detonation wave engines and rocket engines, and may thus be of distinctly different character. In this study we focus on modeling supersonic combustion for dual-mode ramjets and scramjets, in which fuel is almost exclusively injected into a high-speed air-stream passing through the engine, resulting in a non-premixed flame. Non-premixed flames are often, [1], characterized by the flame-structure Damköhler number, $Da_a^fl = \tau_K / \tau_c = (\tilde{\chi}_{st} \tau_c)^{-1}$, in which $\tilde{\chi}_{st}$ is the scalar dissipation rate at stoichiometric conditions, $\tau_c = \delta_u / s_u = \kappa / s_u^2$ the chemical time scale, and κ the thermal diffusivity. For turbulent combustion the values of $Da_a^fl = s_u^2 / (\tilde{\chi}_{st} \kappa)$ determines the flame structure, and for subsonic combustion we discriminate between extinction ($Da_a^fl < Da_a^{ext}$), unsteady ($Da_a^{ext} \leq Da_a^fl \leq Da_a^{lf}$) and flamelet ($Da_a^fl > Da_a^{lf}$) regimes, in which Da_a^{lf} and Da_a^{ext} are the critical laminar and extinction Da-numbers, respectively. For supersonic combustion this picture becomes more complicated as kinetic energy is comparable with sensible enthalpy and dominates over chemical energy, the time scales of flow and chemistry are similar and the flow contains dilatation and shocks possibly affecting the reaction rates.

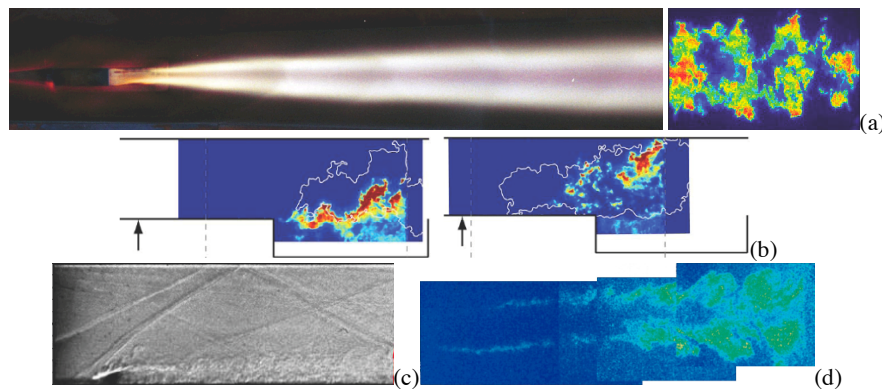


Figure 1. Experimental observations: (a) Spontaneous flame image and cross-sectional OH image from the ONERA-JAXA combustor, [2], using a combined strut injector and flameholder; (b) Instantaneous OH images from cavity- and jet-wake stabilized combustion in a dual-mode ramjet using jet-in-cross-flow injection and cavity based flameholding, [3]; (c) Schlieren images from the ground testing of the HYSHOT combustor, [4], using multiple jet-in-cross-flow injection and aerothermodynamic flameholding, and OH images from the Waidmann scramjet combustor, [5], using a combined strut injector and flameholder

Results from supersonic combustion experiments reveal a somewhat different flame structures than does results from subsonic combustion experiments, figure 1. Most OH or CH₂O PLIF images of supersonic combustion, [2-3, 5], show a fragmented structure, with OH and CH₂O present in pockets following the flow. Schlieren images, [4], reveal the complex relations between a reacting wake, formed behind a transverse fuel injector, and the shock waves traversing the combustor, changing the flow structures and the large scale mixing characteristics, and thus the subsequent chemical reactions. Furthermore, the flame typically stabilizes in a region where the local flow velocity is much higher than the turbulent flame speed but below the ambient air speed, suggesting that supersonic combustion behaves differently from subsonic combustion, in which flame propagation plays a role. Altogether, these results suggest that shock-shock or shock shear-layer interactions couple with chemical reactions to ignite the fuel, resulting in radical species that propagates downstream to the next hot pocket, where further radicals are formed. Once sufficient concentrations have built up, ignition is established and heat release may then occur, even when the mean combustor entry conditions may be too mild for auto-ignition.

2 Overview of Mathematical and Numerical Modeling

The reactive flow equations are the balance equations of mass, momentum and energy describing advection, diffusion and reactions, [6]. As the scales involved in supersonic combustion cover a very wide range, Direct Numerical Simulations (DNS) is usually not an alternative, and modeling appears unavoidable. Reynolds Average Navier Stokes (RANS) models, [7], do not offer an attractive framework as the full range of turbulent scales are modeled together with the turbulence chemistry interactions, [8]. Large Eddy Simulation (LES) models, [9], provide an attractive alternative since in LES the large (energy containing) scales are resolved, whereas only the small, less energetic, scales need to be modeled, [10]. For a linear viscous fluid with Fourier heat conduction and Fickian diffusion the LES equations results from filtering the reactive flow equations so that,

$$\begin{cases} \partial_t(\bar{\rho}) + \nabla \cdot (\bar{\rho} \tilde{\mathbf{v}}) = 0, \\ \partial_t(\bar{\rho} \tilde{Y}_i) + \nabla \cdot (\bar{\rho} \tilde{\mathbf{v}} \tilde{Y}_i) = \nabla \cdot (D_i \nabla \tilde{Y}_i - \mathbf{b}_i) + \bar{w}_i, \\ \partial_t(\bar{\rho} \tilde{\mathbf{v}}) + \nabla \cdot (\bar{\rho} \tilde{\mathbf{v}} \otimes \tilde{\mathbf{v}}) = -\nabla \bar{p} + \nabla \cdot (\mu(\nabla \tilde{\mathbf{v}} + \nabla \tilde{\mathbf{v}}^T) - \frac{2}{3} \mu(\nabla \cdot \tilde{\mathbf{v}}) \mathbf{I} - \mathbf{B}), \\ \partial_t(\bar{\rho} \tilde{E}) + \nabla \cdot (\bar{\rho} \tilde{\mathbf{v}} \tilde{E}) = \nabla \cdot (-\bar{p} \tilde{\mathbf{v}} + \mu(\nabla \tilde{\mathbf{v}} + \nabla \tilde{\mathbf{v}}^T) \tilde{\mathbf{v}} - \frac{2}{3} \mu(\nabla \cdot \tilde{\mathbf{v}}) \tilde{\mathbf{v}} + \kappa \nabla \tilde{T} - \mathbf{b}_E), \end{cases} \quad (1)$$

in which, $\bar{\rho}$, $\tilde{\mathbf{v}}$, \tilde{T} and \tilde{Y}_i are the filtered density, velocity, temperature and species mass fractions, respectively. The filtered pressure is defined as $\bar{p} \approx \bar{\rho} R \tilde{T} \Sigma_i (\tilde{Y}_i / M_i)$ in which R is the (temperature dependent) gas constant and M_i the species molar mass. The mixture is characterized by the viscosity μ , and the species and thermal diffusivities, $D_i = \mu / Sc_i$ and $\kappa = \mu / Pr$, with Sc_i and Pr being the Schmidt and Prandtl numbers, respectively. Furthermore, $\tilde{E} = \bar{h} - \bar{p} / \bar{\rho} + \frac{1}{2} \tilde{\mathbf{v}}^2 + k$ is the total energy, in which $\bar{h} = \Sigma_i (\tilde{Y}_i (h_{i,r}^0 + \int_{T_0}^T C_{p,i}(T) dT))$ is the enthalpy and $k = \frac{1}{2} (\tilde{\mathbf{v}}^2 - \tilde{v}^2)$ the sub grid kinetic energy. The influence of the chemical reactions, $\Sigma_{i=1}^N P_{ij}' \tilde{\mathcal{S}}_i \xrightleftharpoons[k_{r,j}]{k_{f,i}} \Sigma_{i=1}^N P_{ij}'' \tilde{\mathcal{S}}_i$, are through the filtered species reaction rates $\bar{w}_i = M_i P_{ij} \bar{w}_j$, in which $\bar{w}_j = k_j \Pi_{i=1}^N (\rho Y_i)^{P_{ij}}$, with k_i being the (Arrhenius) rate constants, are the reaction rates and P_{ij} the stoichiometric coefficients. The filtering of \bar{w}_j constitutes the main problem in turbulent combustion modeling due to the inherent non-linearity in Y_i and T , requiring rather sophisticated and regime sensitive models for \bar{w}_j . The subgrid flow physics is here concealed in the subgrid terms $\mathbf{B} = \bar{\rho}(\tilde{\mathbf{v}} \otimes \tilde{\mathbf{v}} - \tilde{\mathbf{v}} \otimes \tilde{\mathbf{v}})$, $\mathbf{b}_i = \bar{\rho}(\tilde{\mathbf{v}} \tilde{Y}_i - \tilde{\mathbf{v}} \tilde{Y}_i)$ and $\mathbf{b}_E = \bar{\rho}(\tilde{\mathbf{v}} \tilde{E} - \tilde{\mathbf{v}} \tilde{E})$, [10], that also requires modeling.

The choice of *subgrid flow model*, i.e. the modeling of \mathbf{B} , \mathbf{b}_i and \mathbf{b}_E , seems not critical for most LES, [11], whereas the *subgrid combustion model*, i.e. the treatment of the flame, including the modeling of \bar{w}_j , is very important. Concerning \mathbf{B} , \mathbf{b}_i and \mathbf{b}_E we observe that these terms are not unique to reactive flows, and hence acquire models from the plethora of non-reactive subgrid flow models [10]. The class of Mixed Models (MM), [12-13], $\mathbf{B} = \bar{\rho}(\tilde{\mathbf{v}} \otimes \tilde{\mathbf{v}} - \tilde{\mathbf{v}} \otimes \tilde{\mathbf{v}}) - 2\mu_k \bar{\mathbf{D}}_D$, $\mathbf{b}_i = \bar{\rho}(\tilde{\mathbf{v}} \tilde{Y}_i - \tilde{\mathbf{v}} \tilde{Y}_i) - \frac{\mu_k}{Sc_i} \nabla \tilde{Y}_i$ and $\mathbf{b}_E = \bar{\rho}(\tilde{\mathbf{v}} \tilde{E} - \tilde{\mathbf{v}} \tilde{E}) - \frac{\mu_k}{Pr_i} \nabla \tilde{E}$ have proven extremely reliable due to their functional similarity with the subgrid stress and flux terms, and is here used together with a Smagorinsky eddy viscosity model, [10], and a wall-model, [12], alleviating the requirements of resolving details of the near wall flow physics. Regarding the modeling of the flame, or \bar{w}_j , we may differentiate between *Flamelet Progress Variable* (FPV) and *Finite Rate Chemistry* (FRC), [14], models, both of which can be further divided into additional classes of models depending on further assumptions. The class of FPV models relies on the assumption that

the flame is everywhere thin compared to the flow scales, making it less useful for other flames, or for situations in which the flame can be significantly affected by turbulence or shock-waves.

The modeling of \bar{w}_i should reflect the physics discussed in Section 1, and one way of incorporating this is to divide the flow into fine structures (*) and surroundings (°). The fine-structure regions typically form topologically complex structures, composed of a muddle of interacting tube, ribbon and sheet-like structures in which most of the viscous dissipation and molecular mixing take place. This idea was initially proposed by Chomiak, [15], based on the non-reactive data of Batchelor & Townsend, [16], and was later used by Magnussen to develop the Eddy Dissipation Concept (EDC), [17], and by Sabelnikov & Fureby, [18], to develop an LES version of the Partially Stirred Reactor (PaSR) model. DNS of non-reacting, [19], and reacting, [20], flows support this physical picture of the flow, and reveal that regions of heat-release occur within volumetrically expanding fine-structures. An attribute of the EDC and PaSR models is that the subgrid balance of mass and energy between the surroundings and fine-structures may be expressed as $\bar{\rho}(Y_i^* - Y_i^0)/\tau^* \approx \dot{w}_i(\bar{\rho}, Y_i^*, T^*)$ and $\bar{\rho}\sum_{i=1}^N(Y_i^* h_i^* - Y_i^0 h_i^0)/\tau^* = \sum_{i=1}^N h_{i,f}^0 \dot{w}_i(\bar{\rho}, Y_i^*, T^*)$, in which τ^* and γ^* are the subgrid time-scale and reacting volume fraction. By defining the resolved fields as $\tilde{Y}_i = \gamma^* Y_i^* + (1 - \gamma^*) Y_i^0$ and $\tilde{T} = \gamma^* T^* + (1 - \gamma^*) T^0$, a subgrid model results that is of the form,

$$\begin{cases} \bar{\rho}(Y_i^* - \tilde{Y}_i) = (1 - \gamma^*) \tau^* \dot{w}_i(\bar{\rho}, Y_i^*, T^*), \\ \bar{\rho}\sum_{i=1}^N(Y_i^* h_i^*(T^*) - \tilde{Y}_i \tilde{h}_i(\tilde{T})) = (1 - \gamma^*) \tau^* \sum_{i=1}^N h_{i,f}^0 \dot{w}_i(\bar{\rho}, Y_i^*, T^*). \end{cases} \quad (2)$$

Given τ^* and γ^* from (2) this provides the local thermochemical states of the fine-structures and surroundings, which, in turn can be used to model the filtered reaction rate as,

$$\overline{\dot{w}_j(\rho, T, Y_i)} = \int_{\rho} \int_T \int_{Y_i} \dot{w}_j(\rho, T, Y_i) \dot{w}_j(\rho, T, Y_i) d\rho dT dY_i = \gamma^* \dot{w}_j(\bar{\rho}, T^*, Y_i^*) + (1 - \gamma^*) \dot{w}_j(\bar{\rho}, T^0, Y_i^0). \quad (3)$$

The reacting volume fraction and subgrid time scale may be modeled in different ways: In the LES-EDC model the cascade model, [17], suggests that $\tau^* = \frac{1}{2} \ell^*/v^* \approx 5.0 \tau_K$ and $\gamma^* = (v^*/v')^3$, in which $\ell^* \approx 2.5 \ell_K$ and $v^* \approx v_K$. Since $v' = \frac{2}{3} k^{1/2}$ these expressions can be reformulated using the subgrid quantities (k and μ_k) such that $\gamma^* \approx 1.0 (\mu/\mu_k)^{3/4}$ and $\tau^* \approx 1.2 (\Delta \mu / \bar{\rho} k^{3/2})^{1/2}$, in which $\mu_k = c_k \bar{\rho} \Delta k^{1/2}$. The LES-PaSR model results when γ^* is modeled as $\Delta V^*/\Delta V$, in which ΔV^* is the volume of fine structures (with area ΔS^*) in the volume ΔV (with area ΔS). Based on geometrical considerations, ΔV and ΔV^* may be estimated in terms of the mass flow, \dot{m} , through ΔS^* , resulting in that $\gamma^* \approx \tau_c / (\tau^* + \tau_c)$. Here, the chemical time scale is estimated as $\tau_c = \delta_u / s_u \approx v / s_u^2$, whereas the subgrid time scale is modeled as the geometrical mean of the Kolmogorov time scale, τ_K , and the shear time, $\tau_\Delta = v'/\Delta$, as suggested by the recent DNS, [19], finally resulting in that $\tau^* = (\tau_K \tau_\Delta)^{1/2} = v^{1/4} \Delta^{3/4} v'^{-5/4}$.

The LES equations (1) are most appropriately discretized by Gauss theorem in a finite volume framework for arbitrary cell-shapes. The OpenFOAM C++ library, [21], provides an excellent example of a freely available code framework for solving non-linear systems of partial differential equations like the reactive LES equations. The supersonic combustion cases discussed in Section 3 are all computed using a code based on the OpenFOAM library. In this code, the flux-reconstruction of the convective velocity and scalar fluxes are both based on second order accurate MC interpolation whereas second order accurate linear interpolation is used for all other (viscous and subgrid) fluxes. Time-integration is performed by means of an explicit second order accurate TVD Runge-Kutta scheme, [22]. The code uses a collocated cell-centered variable arrangement, and the equations are solved in a segregated manner with a fixed time step corresponding to a Courant number of 0.3.

3 Validation of Simulation Models and Physics Elucidation

Validation of numerical simulation models for supersonic combustion is more complicated than for conventional combustion due to the lack of complete experimental databases. One case for which a rather complete database is available is the supersonic combustion experiment of Waidmann *et al.*, [5], that previously has been used for validation of both RANS and LES, [23-24]. This configuration consists of a combustor with a slanted upper wall and a combined injector-flameholder, at the base of which H_2 is injected at Ma 1 through a row of 15 holes. Figure 2a presents a side view of the combustor from a LES-PaSR simulation, emulating the combined experimental

schlieren and OH-LIF image in figure 2b. For the LES-PaSR, a hexahedral grid of 12 Mcells is used to discretize a domain with six injectors. LES have also been carried out for a 6 Mcell grid in a narrower domain with three injectors without noticeably influencing the first and second order statistical moments. Both the two-step mechanism [25] and the seven-step mechanism [26] have been used to describe the H₂-air chemistry. From figures 2a and 2b we find that the flow can be divided into an induction zone, where the turbulence determines the mixing and the progress of combustion, a transitional zone dominated by large-scale coherent flow structures, convective mixing and heat-release and a turbulent combustion zone characterized by fully developed turbulent combustion. From the comparisons of axial velocity, $\langle \tilde{v}_x \rangle$, and temperature, $\langle \tilde{T} \rangle$, in figures 2c to 2d it is clear that the seven-step LES-PaSR model outperforms the 2 step LES-PaSR model and the LES-FPV model, [23].

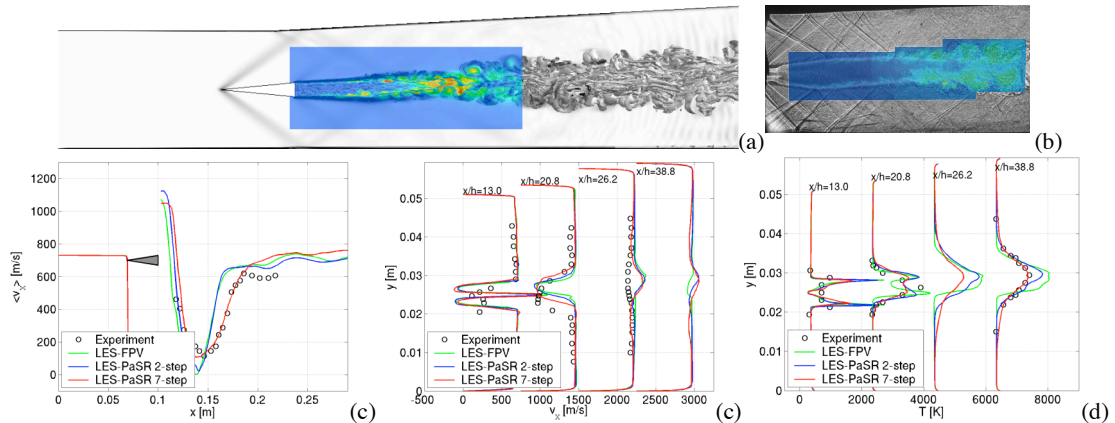


Figure 2. Waidmann combustor: (a) Side view of the flow in terms of the contours of the second invariant of the velocity gradient, gradients of the refraction index and OH mass fraction, (b) experimental OH-LIF and schlieren, (c) centerline axial velocity, (d) axial velocity and (e) temperature at four cross-sections.

Figure 3 presents selected results from predictions of the ONERA-JAXA combustor, [2], (see also figure 1), consisting of a constant area section followed by a diverging area combustor connected to the LAERTE vitiation heater. Hydrogen fuel is injected through three Ma 2.5 injectors located at the strut base and a row of four slanted Ma 2.5 injectors on the top and bottom walls of the strut. The computational model used in [27] spans the entire combustor and is discretized with 9 and 18 Mcells. Experimental and computational flame images, figures 3a and 3a, respectively, shows an expanding flame that separates into an upper and lower branch. From figure 3b it is clear that the shear-layers separating off the strut base break-up into Kelvin Helmholtz (KH) vortices trans-

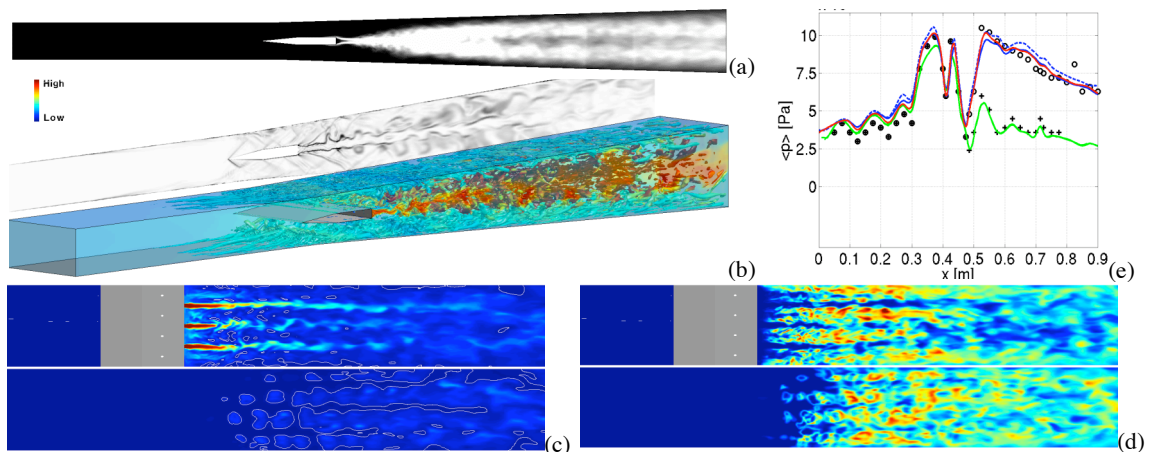


Figure 3. The ONERA-JAXA combustor. (a) Computed flame image, (b) rendering of vorticity colored by temperature from semi-transparent blue to opaque red, (c) mixture fraction, z , and (d) heat release, Q , on the centerplane (top) and two jet diameters above the injection strut (bottom), and (e) pressure at the lower wall. Legend: (+) and (o) non-reacting and reacting experimental data, (—) non-reacting LES, (—) reacting LES-PaSR on coarse grid, (---) reacting LES-PaSR on fine grid and (—) reacting LES-EDC on coarse grid.

ported downstream whilst interacting with neighboring KH structures, the shock-wave pattern, the fuel jets and the flame region, creating a complex flow downstream of the injection strut. The flow is further complicated by the break-up of the H_2 jets, creating vortex structures in the upper and lower shear layers and in the flame region. Figures 3c and 3d shows distributions of the mixture fraction, z , and heat release, \dot{Q} , on the centerplane and two jet diameters above the injection strut, respectively. These distributions agree well with the flame images in figures 1a and 3a. The flame anchors in the high-speed flow zone downstream of the injection strut in a region with intermittent \dot{Q} , containing pockets, showing only a weak correlation with z_{st} , suggesting that the flame does not behave as a traditional diffusion flame. Instead, localized shock-shock and shock shear-layer interactions couple with the chemical reactions to ignite a pocket of sufficiently well mixed fuel-air mixture, resulting in radical species (H, O and OH) being formed that propagates downstream to the next hot pocket, where further radicals are formed. Once sufficient concentrations have built up, ignition is established and heat release occurs, resulting in a speckled \dot{Q} distribution. Figure 3e supports the conjecture that the scramjet combustor is operating as intended and that the time-averaged wall pressure is independent of the spatial resolution.

A more realistic scramjet engine configuration is the HyShot II combustor, [28], for which both laboratory, [4], and flight-test results, [29], exists together with RANS and LES predictions, [30-31]. Figure 4a shows selected aspects of the flow in the HyShot II combustor predicted by LES-PaSR with 12.5 Mcells, [31]. The wall pressure (i) shows that the pressure increases linearly with increasing distance from the H_2 jets up to ~ 30 jet diameters, whereafter it suddenly increase rapidly up to ~ 60 jet diameters to peak at ~ 100 jet diameters. High wall pressures are also found beneath the bow shock, forming a hood over the transverse fuel jet and beneath the fuel jets. The color-coded vortex structures in (ii) and (iv) reveal that the transverse H_2 jets consist of S-shaped side-arm vortices with their lower parts aligned with the flow and their upper parts curling over the H_2 jet forming the neck (circumferential rollers) of the counter-rotating vortex pair, also found by Ben Yakhar *et al.*, [32]. These structures arise from KH instabilities in the jet shear layers beneath the bow-shock, and dominate the fuel-air mixing process during the first 10 to 40 jet diameters. Self-ignition starts once the fuel-air mixture is sufficiently well mixed, and is triggered by hot-spots in regions of colliding shocks which hence explains the unsteady nature of the self-ignition region. Comparing the predicted and measured wall pressures in figure 4b shows that the LES-PaSR computation better captures the experimental sigmoidal pressure profile than does the RANS-PDF computation, [30], and the main difference between these predictions appears to be the ability of the LES model to capture the unsteady mixing, self-ignition and combustion dynamics.

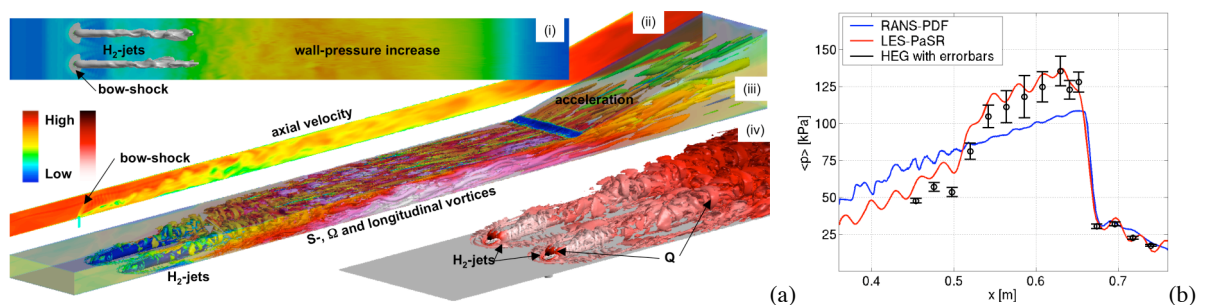


Figure 4. The HyShot II scramjet at 32.5 km altitude. (a) Composite figure of the reacting flow showing (i) wall pressure and an iso-surface of the H_2 mass fraction, (ii) axial velocity through a fuel injector, (iii) iso-surface of the second invariant of the velocity gradient, λ_2 , colored by temperature and (iv) iso-surfaces of the H_2 mass fraction (gray) and the heat release conditioned on λ_2 . (b) Centerline wall pressure distribution.

4 Concluding Remarks

In this paper a comprehensive review of supersonic combustion modeling have been provided from the authors perspective and experience. Here, we focus on modeling supersonic combustion for dual-mode ramjets and scramjets, in which fuel is almost exclusively injected into a supersonic air-stream through the engine, resulting in a non-premixed flame. The ability to model supersonic combustion, as well as ordinary combustion, requires the model to be based on LES in order to resolve the unsteady flow features together with a reasonably accurate reaction mechanism that can describe the major species. Based on our experience, LES-EDC or PaSR models,

founded on an underlying heterogeneous multi-scale description of the balance of energy and species concentrations, are the most appropriate subgrid combustion models to use as they conceptually mimic the underlying fragmented flow structures. In the results discussed it is clear that these models also provides the best qualitative and quantitative agreement with the experimental data. The computations discussed are also used to describe the underlying physics of mixing, self-ignition, flameholding and turbulent combustion.

Acknowledgement

The contributions of V.S. and C.F was supported by the Office National d'Etudes et de Recherches Aeronautiques, France and the Swedish Armed Forces, respectively. The authors thank Sebastian Karl, Klaus Hanneman and Michael Oswald for many fruitful discussions and for providing data and information.

References

- [1] Veynante D. & Vervisch L.; 2002, *Prog. Energy. Comb. Sci.*, **28**, p 193.
- [2] Sunami T., Magré P., Bresson A., Grisch F., Orain M., & Kodera M.; 2005, AIAA 2005-3304,
- [3] Micka D.J. & Driscoll J.F.; 2010, "Reaction Zone Structure in a Laboratory Dual-mode Scramjet Combustor From Simultaneous OH/CH₂O - PLIF", 6th Mediterranean Combustion Symposium.
- [4] Schramm J.M., Karl S., Hannemann K & Strelant J.; 2008, AIAA 2008-2547.
- [5] Waidmann W., Alff F., Brummund U., Böhm M., Clauss W. & Oswald M.; 1995, *Space Tech.* **15**, p 421.
- [6] Oran E.S. & Boris J.P.; 2001, "Numerical Simulation of Reactive Flow", Cambridge University Press, Cambridge, UK.
- [7] Girimaji S.S.; 1991, *Comb. Sci. Tech.*, **78**, p 177.
- [8] Oefelein J.C., Drozda T.G. & Sankaran V.; 2006, *J. Phys.: Conf. Ser.*, **46**, p 16.
- [9] Fureby C.; 2009, *Phil. Trans. R. Soc. A*, **367**, p 2957.
- [10] Sagaut P.; 2001, "Large Eddy Simulation for Incompressible Flows", Springer Verlag, Heidelberg.
- [11] Svennberg U. & Fureby C.; 2010, AIAA 2010-0012.
- [12] Bensow R. & Fureby C., 2006, *J Turbulence* **8**, p N54.
- [13] Speziale C.G., Erlbacher G, Zang T.A. & Hussaini M.Y.; 1988, *Phys. Fluids*, **31**, p 940.
- [14] Fureby C.; 2007, AIAA 2007-1413.
- [15] Chomiak J.; 1979, *Progress Energy Comb. Sci.*, **5**, p 207.
- [16] Batchelor G.K. & Townsend A.A.; 1947, *Proc. Roy. Soc. London Ser A*, **190**, p 534.
- [17] Magnussen B.F., 1981, 19th AIAA Sc. Meeting, St. Louis, USA, p. 213.
- [18] Sabelnikov V. & Fureby C.; 2011, "LES Combustion Modeling utilizing a Multi-Phase Analogy", In preparation for Combustion Modeling & theory.
- [19] Yeung P.K., Pope S.B. & Sawford B.L.; 2006, *J. Turbulence*, **7**, N58.
- [20] Tanahashi M., Fujimura M. & Miyauchi T.; 2000, *Proc. of the 28th Int Symp on Comb*, p 5729.
- [21] Weller H.G., Tabor G., Jasak H. & Fureby C.; 1997, *Comp. in Physics*, **12**, p 629.
- [22] Gottlieb S. & Shu C.-W.; 1998, *Mathematics of Computation*, **67**, p 73.
- [23] Berglund M. & Fureby C.; 2006, 31st Int. Symp on Comb., p 2491.
- [24] Genin F. & Menon S.; 2009, AIAA 2009-0132.
- [25] Rogers R.C. & Chinitz W.; 1982, AIAA 1982-0112.
- [26] Davidenko D.M., Gökalp I., Dufour E. & Magre P.; 2006, AIAA 2006-7915.
- [27] Berglund M., Fedina E., Fureby C., Sabel'nikov V. & Tegnér J.; 2010, *AIAA.J.*, **48**, p 540.
- [28] Paull A., Alesi, H. & Anderson, S.; 2002, AIAA 2002-4939.
- [29] Smart M.K., Hass N.E. & Paull A.; 2006, *AIAA J.*, **44**, p 2366.
- [30] Karl S., Hannemann K, Strelant J. & Mack A.; 2006, AIAA 2006-8041.
- [31] Fureby C., Chapuis M., Fedina E. Karl S.; 2010, "CFD Analysis of the Hyshot II Combustor", *Proc. of the Comb. Inst.*, **33**, doi:10.1016/j.proci.2010.07.055.
- [32] Ben-Yakar A., Mungal M.G. & Hansen R.K.; 2006, **18**, p 026101.